Published in final edited form as:

Biol Psychiatry. 2023 July 01; 94(1): 68–83. doi:10.1016/j.biopsych.2022.11.016.

Excessive protein accumulation and impaired autophagy in the hippocampus of Angelman syndrome modeled in mice

Francesca Aria[1,#], **Kiran Pandey**[1,#], **Cristina M. Alberini**[1,*]

[1]Center for Neural Science, New York University, New York, NY, USA 10003

Abstract

Background: Angelman syndrome (AS), a neurodevelopmental disorder caused by abnormalities of the 15q11.2-q13.1 chromosome region, is characterized by impairment of cognitive and motor functions, sleep problems, and seizures. How the genetic defects of AS produce these neurological symptoms is unclear. Mice modeling AS (AS mice) accumulate activity-regulated-cytoskeleton-associated protein (ARC/ARG3.1), a neuronal immediate early gene (IEG) critical for synaptic plasticity. This accumulation suggests an altered protein metabolism.

Methods: Focusing on the dorsal hippocampus (dHC), a brain region critical for memory formation and cognitive functions, we assessed levels and tissue distribution of IEGs, *de novo* protein synthesis, and markers of protein synthesis, endosomes, autophagy, and synaptic functions in AS mice at baseline and following learning. We also tested autophagic flux and memory retention following autophagy-promoting treatment.

Results: AS dHC exhibited accumulation of IEGs ARC, FOS, and EGR1, autophagy proteins MLP3B, SQSTM1, and LAMP1, and reduction of the endosomal protein RAB5A. AS dHC also had increased levels of *de novo* protein synthesis, impaired autophagic flux with accumulation of autophagosome, and altered synaptic protein levels. Contextual fear conditioning significantly increased levels of IEGs and autophagy proteins, *de novo* protein synthesis, and autophagic flux in the dHC of normal mice, but not in AS mice. Enhancing autophagy in the dHC alleviated AS-related memory and autophagic flux impairments.

Conclusions: A major biological deficit of AS brain is a defective protein metabolism, particularly that dynamically regulated by learning, resulting in stalled autophagy and accumulation of neuronal proteins. Activating autophagy ameliorates AS cognitive impairments and dHC protein accumulation.

Keywords

Angelman Syndrome; mouse; autophagy; protein synthesis; immediate early genes; hippocampus

[*]Correspondence should be addressed to: Cristina M. Alberini, Center for Neural Science, New York University, 4 Washington Place, New York, NY, 10003, ca60@nyu.edu; Phone: 212-998-7721.
[#]These authors equally contributed

Introduction

Angelman Syndrome (AS) is a genetic neurodevelopmental disorder caused by defects of the 15q11.2-q13.1 chromosomal region, which in neurons is paternally imprinted (1,2). Most AS cases have deletions or mutations of the gene encoding the ubiquitin-protein ligase E3A (UBE3A), a critical player of the ubiquitin-proteasome system --a protein degradation system involved in neuronal morphological maturation, synaptic plasticity, and cortical development (3,4).

AS presents with developmental delay, intellectual disability, speech impairment, movement and balance deficits (ataxia), and seizures (5). How the AS genetic defects cause brain dysregulations resulting in those neuropsychiatric symptoms is still unclear. AS is associated with neuronal accumulation of the immediate early gene (IEG) product activity-regulated cytoskeleton-associated protein (ARC/ARG3.1; hereafter ARC) (6,7), which plays important roles in synaptic plasticity and memory by controlling endocytosis of α-amino-3-hydroxy-5-methy1-4-isoxazolepropionic acid receptors (AMPARs) (8-10) and via intercellular communication (11). Hence, ARC accumulation may contribute to the dysregulation of synaptic functions found in AS brain (12). ARC is a target of UBE3A-mediated ubiquitination, but it is debated whether its accumulation in AS neurons results from defective ubiquitin-mediated degradation (6) or impaired autophagy (13, 14) --the other major protein degradation process that targets proteins to lysosomal degradation via autophagosomes (15). E3 ubiquitin protein ligases might be involved in the regulation of autophagy (16). Also there is evidence showing that a target of UBE3A, huntingtin-associated protein 1 (HAP1), a protein that promotes autophagosome transport and is dysregulated in Huntington's disease (HD) (17), accumulates in AS mouse brain (18), suggesting that both the ubiquitin and autophagy systems may be altered in AS neurons. Yet, it remains to be understood whether autophagy is increased or decreased in AS brain and particularly whether autophagy regulated following learning is altered in AS brain. Learning leads to an upregulation of autophagy that is critical for the formation of long-term memory (19-21). This autophagy increase is coupled to the increase in *de novo* protein synthesis evoked by learning, via the synthesis of autophagy proteins, including microtubule-associated protein 1 light chain 3 beta (MLP3B, also known as LC3B), sequestosome-1 (SQSTM1, also known as p62), and lysosome-associated membrane glycoprotein 1 (LAMP1) (21). Learning-induced autophagy also requires ARC (21).

These protein metabolism regulations induced by learning and required for long-term memory formation led us hypothesize that AS could be associated with alterations of protein metabolism in the brain and, in particularly with alterations of learning-dependent processes. To test this hypothesis, we used a widely-employed model of AS in mice, which lacks a functional maternal allele of UBE3A (Ube3a m^{-}/p^{+} mice; 22) and conducted behavioral assessments along with biochemical, immunohistochemical, and bio-functional assays on the dorsal hippocampus (dHC), a brain region that is critical for memory and cognitive functions (23). The AS mice recapitulate the genetics of human patients and exhibit most core phenotypes of the disease, including cognitive impairments (24-35), hence they represent a clinically-relevant rodent model of AS (36). As several laboratories validated that

AS mice have impaired contextual fear conditioning (CFC) (22,30-35), we employed this learning paradigm in our studies.

Methods and Materials

Mice

All the studies were performed on adult male and female maternal *ube3a*-deficient mice (Ube3a m^{-}/p^{+} or AS mice) and littermates wild-type (WT) controls of approximately 8 weeks of age at the start of experiments. All data shown in the present study included both female and male mice. Detailed protocols are provided in Supplement 1.

Contextual fear conditioning (CFC) and immediate shock (IS) control paradigm were performed as previously described (35,37). Detailed methods are reported in Supplement 1.

Cannulae implants targeting the dHC of mice and bilateral injections of TAT-Beclin 1 and SBI-0206965 (SBI) or vehicle were performed as described previously (38). Detailed protocols are described in Supplement 1.

***In vivo* surface sensing of translation (SUnSET)** was carried out as previously described (38,39). The detailed protocol is described in Supplement 1.

RNA isolation followed by quantitative polymerase chain reaction (qPCR) analyses was carried out as described previously (21). The detailed protocol is described in Supplement 1.

Hippocampi dissection, protein extraction, synaptoneurosomal preparation, and western blot analyses were carried out as previously described (38-40). The detailed protocols are described in Supplement 1.

Immunohistochemistry, confocal imaging, and analyses of autophagy markers (MLP3B, SQSTM1, LAMP1) and ARC were done as previously described (21) and detailed protocols are reported in Supplement 1.

Autophagic flux measurements were performed as previously described (21) and the detailed protocol is reported in Supplement 1.

Statistical analyses were performed as described in Materials and Methods in Supplement 1. See Table 1-3 in Supplement 1 for detailed description of statistical analyses used in each experiment.

Results

Accumulation and impaired learning-dependent regulation of IEG products in the hippocampus of AS mice

ARC levels are elevated in cultured activated neurons of AS mice and particularly in their dendritic compartment (7). Here we employed qPCR and western blot analyses to determine the mRNA and protein levels of the IEGs ARC, c-Fos (FOS), and early growth response protein 1 (EGR1) in the dHC of young adult AS mice and wild-type littermate controls

(WT) in both untrained conditions and following contextual fear conditioning (CFC). These IEGs are rapidly transcribed and translated in response to learning and are considered markers of neural activation (41). QPCR analyses showed that in untrained conditions the mRNA levels of *Arc, Fos, and Egr1* in the dHC of AS and WT mice were similar. CFC significantly increased the IEG mRNA levels in both WT and AS mice compared to their respective untrained controls, although the increases in AS were less pronounced than those of WT mice (Figure 1A). In contrast, western blot analyses revealed that the levels of ARC, FOS, and EGR1 proteins in untrained conditions were significantly higher in AS mice compared to WT littermates. CFC significantly increased the IEG levels in WT mice (41-43), but not in AS mice (Figure 1B, Figure S1). Immunohistochemical staining revealed that the accumulation of ARC in the dHC of AS mice occurred throughout all subregions. Quantifications performed in CA1 and *dentate gyrus* (DG) highlighted significant ARC increase in both (Figure 1C, Figure S2). Furthermore, qualitative morphological assessment indicated that ARC accumulated in all subcellular compartments: nucleus, soma, and processes, and its distribution appeared similar to that typically observed in the dHC of trained rats and mice (Figure 1C, Figure S2) (40,44). Finally, in agreement with the western blot data, whereas CFC in WT mice evoked the typical significant increase in ARC level in dHC, no changes were detected in AS mice, neither in ARC level nor in its subcellular distribution (Figures 1C, Figure S2).

We concluded that, while the IEG mRNA levels and learning-dependent increase are similar in the dHC of AS and WT mice, the IEG protein levels are significantly higher in AS mice and do not change following learning. As increased protein levels could be explained by either higher synthesis or impaired degradation, we proceeded to investigate these processes.

The dHC of AS mice has an increased rate of *de novo* protein synthesis, which does not change following learning

Using western blot analyses, we quantified the dHC levels of the following key proteins critical for the regulation of mRNA translation: phosphorylation at Ser2448 of protein kinase mammalian target of rapamycin (p-MTOR, 45), phosphorylation at Ser240/244 of ribosomal protein S6 (p-RS6), which is considered a read out of activity-dependent mRNA translation (46-49), the levels of the cap-binding eukaryotic translation initiation factor 4E (IF4E) protein and of the translational repressor eukaryotic translation initiation factor 4E-binding protein 2 (4EPB2), both considered rate limiting steps for the translation of most mRNAs (50-54).

AS and WT mice had similar levels of p-MTOR and MTOR, but AS mice had a significantly higher p-RS6 levels with similar RS6 levels, hence a significantly higher p-RS6:RS6 ratio, suggesting that AS dHC had an increased basal mRNA translation. AS mice also displayed a significant increase in IF4E, despite 4EBP2 levels were similar in the two groups (Figure 2A-C).

CFC, which is well-known to evoke a rapid increase in *de novo* protein synthesis (55,56), led to a significant elevation, at 1 hour after training, of both p-RS6 and IF4E in the dHC of WT mice relative to untrained WT controls, without changing p-MTOR, MTOR, RS6 and 4EBP2 levels (Figure 2A-C, Figure S1). In contrast, in AS mice, CFC failed to elicit

any change, suggesting that their dHC had a defective learning-dependent mRNA translation (Figure 2A-C).

Next, we assessed the global rate of *de novo* protein synthesis in the dHC using *in vivo* surface sensing of translation (SUnSET, 38,39). SUnSET was measured at 1 hour both in untrained conditions as well as following CFC to assess the rapid induction of protein synthesis following learning, which is a fundamental requirement for long-term plasticity and memory (57,58). In untrained conditions, AS mice showed a significantly increased level of *de novo* protein synthesis relative to WT (Figure 2D, Figure S1). Protein synthesis significantly increased upon CFC in WT (39), but not in AS mice (Figure 2D). Thus, AS mice have an enhanced rate of *de novo* protein synthesis in the dHC under basal conditions and lack the dynamic induction of mRNA translation typically evoked by learning and necessary for long-term plasticity and memory formation.

Levels of proteins involved in autophagy and their learning-dependent regulations are altered in the dHC of AS mice

MTOR also plays a key role in autophagy, thus, maintaining growth balance (59,60). MTOR and the energy detector AMP-activated protein kinase (AMPK) regulate autophagy by phosphorylating the autophagy-initiating kinase UNC-51-like kinase 1 (ULK1) at different sites and leading to either inhibition or activation of autophagy, respectively (61,62). Phosphorylation of ULK1 at Ser777 (p-ULK1), mediated by AMPK, phosphorylates BECLIN-1 (BECN1) at Ser14, resulting in its activation, a critical step required for the initiation of autophagy (63). Although still understudied, some mechanisms link autophagy with endocytic pathways; for example, BECN1 is implicated also in endosome vesicle trafficking (64,65) and endocytosis is regulated by ARC (8). Endosomes sort proteins and lipids of the secretory and endocytic pathway (66). Distinct populations of endosomes are defined by specific proteins: the early endosomal antigen 1 (EEA1) and Ras-related protein Rab-5A (RAB5A) are markers of early endosomes (EE) (67-69), while Ras-related protein Rab-7a (RAB7A) marks late endosomes (LE) and is involved in autophagy maturation (70) (see schema in Figure 3A). Using western blot analyses, we assessed p-AMPK (phosphorylation of AMPK at Thr172, a marker of AMPK activation, 71), AMPK, p-ULK1, p-BECN1, BECN1, EEA1, RAB5A, RAB7A, to determine whether AS dHC has alterations in autophagy and/or endosomal markers.

As depicted in Figure 3A, relative to WT, AS mice had significantly higher levels of p-AMPK and similar levels of AMPK, hence a significantly higher p-AMPK:AMPK ratio. AS mice also had significantly reduced p-ULK1 and p-BECN1, but similar levels of BECN1, hence significantly lower p-BECN1:BECN1 ratio, suggesting that they have an impaired initiation of autophagy. Relative to untrained conditions, CFC increased the levels of p-AMPK and p-BECN1 in the dHC of WT mice without changing AMPK and BECN1 levels, and therefore increased p-AMPK:AMPK and p-BECN1:BECN1 ratios. In contrast, no changes were found following CFC in the dHC of AS mice relative to their untrained controls (Figure 3A, Figure S3). Hence initiation of autophagy, in both untrained conditions and following learning, seemed to be impaired in AS mice.

RAB5A was significantly lower in AS compared to WT, whereas the levels of EEA1 and RAB7A were similar in both groups (Figure 3B, Figure S3). CFC significantly increased EEA1 level in WT mice without changing RAB5A and RAB7A levels (Figure 3B). In contrast, none of the endosomal markers changed with training in AS mice, indicating that, in addition to a defective autophagy initiation, the dHC of AS mice has altered EE pools and fails to regulate EE functions in response to learning.

The training-induced molecular changes found in the WT dHC were selective for associative learning as an immediate shock experience (IS), a paradigm that does not elicit associative CFC memory (37), failed to induce any change in the levels of IEGs, and of mRNA translation, autophagy, and endosomal markers in the dHC of WT as well as AS mice (Figure S4).

To better characterize the autophagy alterations in AS mice we investigated additional autophagic markers (Figure 3A). Learning increases autophagy and lysosomal protein levels (19-21), including MLP3B, a marker of autophagosomes (72), SQSTM1, which directs ubiquitinated proteins to autophagosomes (73,74), and LAMP1, a marker of acidic vesicles including lysosomes (75). Learning also elevates autophagic flux (21), a measure of the degradative capacity of autophagosomes (76). All these increases require *de novo* protein synthesis and ARC (21). Here we assessed autophagy markers under basal conditions and at 1 hour following CFC in the dHC of AS and WT mice. Using a western blot protocol that reliably detects MLP3B-I and -II in brain extracts (see Supplement 1 and 21), we determined the levels of MLP3B-I:MLP3B-II ratio, a readout of autophagic activity (77-79). We found that the levels of both proteins were significantly higher in AS mice relative to WT (Figure 3C, Figure S3). Compared to untrained conditions, CFC significantly increased MLP3B-II levels and the ratio of MLP3B-II: MLP3B-I in WT mice but not in AS mice (Figure 3C, Figure S3).

Immunohistochemical analyses showed that AS mice had a significantly higher levels of MLP3B, SQSTM1, and LAMP1 in both CA1 and DG (Figure 4). Moreover, relative to untrained conditions, CFC significantly increased these proteins in WT mice but not in AS mice (Figure 4).

In sum, the dHC of AS mice had an accumulation of autophagy proteins and a reduction of some EE and of autophagy initiation markers, suggesting a defective autophagy. To test this hypothesis we proceeded to assess *in vivo* dHC autophagic flux.

Autophagic flux is impaired in the hippocampus of AS mice

To measure autophagic flux in the dHC of AS and WT mice, we bilaterally injected adeno-associated virus (AAV) containing mCherry-GFP-LC3B, an *in vivo* pH-sensitive reporter of autophagic flux (21,80). While GFP is acid-sensitive, mCherry is acid-resistant, hence the double-tagged mCherry-GFP-LC3B–labeled autophagosomes appear as yellow puncta in non-acidic compartments and as red puncta in acidic vesicles. Thus, comparative immunofluorescence assessment of the ratio of red:yellow puncta number provides a measure of the relative autophagic flux (80).

Two weeks after AAV infection showed reliable and strong expression of mCherry-GFP-LC3B in the dHC of mice (Figure 5). A qualitative assessment of the fluorescence showed the presence of: i) dispersed puncta throughout the dHC (Figure 5B and 5D, Figure S5A) (*dispersed puncta*) and ii) puncta in a population of highly transduced cells with bright cell body fluorescence (Figure 5C and 5E, Figure S5B) (*bright cell puncta*). Furthermore, AS but not WT mice also had iii) enlarged fluorescent structures (*aggregates*) throughout the dHC, which emerged after setting a puncta size exclusion measure that subtracted all the puncta size present in WT (see Supplement 1). We quantified the flux of dispersed puncta, bright cell puncta, and aggregates in the CA1 and DG subregions of WT and AS mice in untrained conditions and at 1 hour after CFC by measuring the number of yellow and red MLP3B puncta, the ratio of red:yellow MLP3B puncta, the average puncta size, and the percentage of aggregates. To assess rate of infectivity in all groups we also quantified the percentage of bright fluorescent cells in the CA1 and DG subregions relative to the total number of cells measured by DAPI staining within a set dHC area. We found similar percentage of bright cells across all groups indicating that they had similar rates of viral infection (Figure 5C and 5E).

As shown in Figure 5B and 5D, under basal conditions, the number of yellow puncta was significantly higher in both CA1 and DG of AS mice compared to WT controls. Of the total number of yellow puncta, 15.87± 1.08% in CA1 and 8.67 ± 0.58% in DG emerged as aggregates (Figure 5B and 5D, Figure S5A). This accumulation of autophagosomes (LC3B-labelled) in aggregates was also reflected by the significantly larger average puncta size in both CA1 and DG of AS mice relative to the average puncta size of autophagosome in WT controls (Figure 5B and 5D). The presence of aggregates suggested a stalled autophagic flux in AS mice. Analyses of the bright cell puncta number also showed impaired autophagic flux in both CA1 and DG of in AS mice (Figure 5C and 5E, Figure S5B), but no aggregates were found in these cells, hence their average puncta size was not significantly different from that of WT mice (Figure 5C and 5E).

Relative to untrained conditions, CFC significantly increased autophagic flux in CA1 and DG of WT mice, along with a significant increase in red puncta size (Figure 5C, 5E and S5). In contrast, AS mice did not change any of these parameters (Figure 5B, 5E, and S5); however, they had a significant decrease in the number of aggregates (Figure 5B and 5D, Figure S5A) and consequently of average puncta size (Figure 5B and 5D), suggesting that training increased to some degree autophagic flux in AS dHC.

In sum, compared to WT, AS dHC had a higher number of autophagosomes and formed large aggregates of phagosomal structures, evidence of impaired autophagy. While learning significantly increases autophagic flux in WT mice, it failed to do so in AS mice. However, learning decreased to some extend the number of aggregates in AS mice.

AS mice have reduced levels of pre-synaptic markers and increased post-synaptic levels of GRIA1 and SYGP1 in the dHC

AS neurons have abnormal synaptic plasticity, dendritic spine morphology, and decreased dendritic spine density (26,81,82). They also have altered phosphorylation of calcium/calmodulin-dependent protein kinase type II subunit alpha (CaMKIIα) (83), a protein

that regulates synaptic transmission, synaptic plasticity, and memory formation by phosphorylating pre-and post-synaptic proteins (84-86). Hippocampal neuronal cultures of AS mice also have decreased plasma membrane levels of glutamate ionotropic receptor AMPA type subunit 1 (GRIA1) (6).

Synaptic protein levels are regulated in response to learning and plasticity stimuli by a coordinated process of protein synthesis and degradation, including autophagy (87,88). Autophagosome formation in presynaptic compartments is important for synaptic transmission regulation and post-synaptic functions (89). Given the defective protein metabolism regulations found in AS dHC, here we used western blot analyses to assess their levels of pre- and post-synaptic proteins. We compared protein extracts from total dHC and synaptoneurosomal fractions (SN) obtained from WT and AS dHC (see Figure S6A for biochemical validation of SN fractionation). The total protein extract yield was similar in WT and AS. In contrast, SN protein yield was significantly higher in AS mice (Figure S6B and S6C), suggesting protein accumulation at synapses. Similar protein yields were found in both total and SN extract of trained WT and AS mice (Figure S6B).

We determined the levels of the presynaptic proteins synapsin-1 (SYN1) and synaptophysin (SYPH), which are critical for synaptic neurotransmitter release (90,91) and contribute to synaptogenesis and neuronal plasticity (92,93) as well as the phosphorylation of SYN1 at Ser603 (p-SYN1), which is involved in synaptic vesicle release (94). The total protein extracts from AS mice showed a significant reduction in the levels of p-SYN1, SYN1 and SYPH relative to WT controls (Figure 6A, Figure S1 and S3). CFC did not change the levels of p-SYN1, SYN1 and SYPH in WT mice but increased the levels of p-SYN1 and SYN1 in AS mice, relative to their untrained controls (Figure 6A, Figure S1 and S3). No changes in the levels of the pre-synaptic markers were found in the SN of WT and AS mice, neither in untrained conditions nor following CFC (Figure 6A). Although no changes were found in SN fractions, the changes found in the total protein extracts suggested that the dHC of AS mice have significant alterations in mechanisms of neurotransmission.

We then assessed levels of postsynaptic proteins, especially proteins known to be regulated or interacting with ARC and involved in receptor trafficking, i.e, the AMPA receptor subunits GRIA1 and GRIA2, postsynaptic density protein 95 (PSD-95), and the Ras/Rap GTPase-activating protein SynGAP1 (SYGP1) (7,95,96). ARC regulates homeostatic synaptic scaling by removing AMPA receptors from the synaptic membrane (8,10) and by negatively regulating their transcription (97). The trafficking and clustering of AMPA receptors is regulated by PSD-95, which controls formation and maturation of new excitatory synapses (98,99) and by SYGP1 (100,101). Western blot analyses of total dHC protein extracts revealed that, relative to WT, AS mice had a significant increase in the levels of GRIA1 and SYGP1, and a trend towards a decrease in PSD-95, which however was not statistically significant (Figure 6B, Figure S1 and S3). CFC did not affect the levels of any of these proteins in WT or AS mice, relative to their respective untrained controls (Figure 6B, Figure S1 and S3). No difference was found between the total protein extracts of AS and WT for GRIA2 in both untrained conditions and following training. Similar to their total extract, the SN fraction of AS mice had a significant increase in SYGP1 relative to WT (Figure 6B, Figure S1 and S3). No changes were detected in the SN levels of the other

post-synaptic proteins investigated. CFC did not change the levels of these proteins in the SN fraction in either WT or AS mice (Figure 6B, Figure S1 and S3).

We concluded that the dHC of AS mice, compared to WT, has alterations in both pre- and postsynaptic proteins, in particular a decrease in presynaptic proteins such as SYPH, SYN1, and p-SYN1 and an accumulation of postsynaptic proteins such as GRIA1 and SYGP1.

Promoting autophagy attenuates the memory and autophagy impairments of AS mice

We tested whether pharmacological treatments that either promote or inhibit autophagy affect CFC memory formation in both AS and WT mice. Toward this end, we injected bilaterally into the dHC 15 minutes before training either TAT-Beclin 1 peptide to promote autophagosome formation (20,102), or SBI-0206965 (SBI) to selectively block ULK1 phosphorylation thus preventing autophagy initiation (103). TAT-Beclin 1 significantly increased memory in WT mice, a result in agreement with previous studies (20) and significantly reversed the CFC impairment of AS mice, restoring performance to the level of vehicle-injected WT mice (Figure 7). WT mice injected with TAT-Beclin 1 showed a significantly higher memory relative to TAT-Beclin 1-injected AS mice. In contrast, bilateral dHC SBI injection impaired CFC retention in WT mice and had no effects on the impaired CFC in AS mice, relative to respective vehicle-injected controls (Figure 7). Thus, promoting autophagy ameliorates memory impairments of AS mice.

We then tested whether TAT-Beclin 1 affected autophagic flux. WT and AS mice, expressing mCherry-GFP-LC3B in the dHC, were bilaterally injected with TAT-Beclin 1 or scrambled peptide into the dHC 15 minutes before CFC. Autophagic flux was assessed 1 hour after training by analyzing the flux parameters in dispersed puncta, bright cell puncta, and aggregates in both CA1 and DG subregions (Figure 8, Figure S7 and S8). Similar number of bright cells were detected in either subregion of all groups of mice indicating similar rates of infection (Figure 8B and 8D).

In WT mice, relative to scrambled peptide, TAT-Beclin 1 led to a trend towards an increase in autophagic flux, which however did not reach statistical significance (Figure 8). In AS mice, TAT-Beclin 1 significantly increased autophagic flux in both CA1 and DG (Figure 8) and significantly reduced the percent of aggregates (CA1: Scrambled-injected group = 14.95 ± 1.22%; TAT-Beclin 1-injected group = 5.99 ± 0.23%, and DG: Scrambled-injected group = 9.39 ± 0.74%; TAT-Beclin 1-injected group = 2.41 ± 0.16%), hence significantly decreasing the average puncta size (Figure 8A and 8C). TAT-Beclin 1 also significantly enhanced autophagic flux in the bright cells of untrained AS mice but had no effect in WT controls (Figure 8B and 8D). In the bright cells of AS mice, TAT-Beclin 1 did not change the average puncta size, neither in CA1 nor in DG (Figure 8B and 8D), indicating that the reduction of average puncta size in AS was mostly due to a reduction in the number of aggregates.

CFC, as expected, significantly increased the autophagic flux in WT mice but failed to do so in AS mice in both CA1 and DG subregions (Figure 8). TAT-Beclin 1 further increased autophagic flux of both dispersed and bright cell puncta in WT mice (Figure 8, Figure S7 and S8) but did not further change any of these parameters in AS mice. However,

TAT-Beclin 1 significantly reduced the number and size of aggregates in both CA1 and DG of trained AS mice (Figure 8A and 8C). We concluded that TAT-Beclin 1 amelioration of CFC memory deficits in AS mice is accompanied by an increase in autophagic flux.

Discussion

We showed that maternal ube3a deletion, which is typical of AS, is associated with alterations of protein metabolism mechanisms in the dHC. Specifically, the dHC of AS mice had: i) increased rate of *de novo* protein synthesis, ii) accumulation of the IEGs ARC, FOS, and EGR1 and the autophagy proteins MLP3B, SQSTM1, and LAMP1, iii) altered levels of autophagy initiation markers, i.e, increased p-AMPK and decreased p-ULK1, iv) impaired autophagic flux and accumulation of autophagosomal aggregates, v) higher total protein yield in SN extracts, vi) significant decrease of the endosomal trafficking proteins p-BECN1 and RAB5A and of presynaptic proteins p-SYN1, SYN1 and SYPH, and, vii) significant increased levels of the post-synaptic proteins GRIA1 and SYGP1. Moreover, viii) the learning-evoked increases in dHC *de novo* proteins synthesis, IEG levels, and autophagic flux typically found in healthy mice were not observed in AS mice. Finally, ix) promoting autophagy with TAT Beclin 1 in AS dHC partially reversed memory and autophagy impairments and decreased autophagic aggregate levels, suggesting that the amelioration of AS-related symptom is linked to increased autophagy.

Collectively, these data lead us to propose that AS has neuronal dysregulations of vesicle-mediated functions, including endosomal functions, protein synthesis perhaps taking place of endosomal vesicles (104), and autophagy (Figure 9). We suggest that defective vesicle-mediated flux, and particularly autophagic flux is at the root of the inability of AS brain to dynamically regulate protein metabolism in response to activations, such as that evoked by learning. These alterations with consequent protein accumulations in brain circuitries likely lead to synaptic plasticity impairment with consequent behavioral dysfunctions. The dHC is likely not the only region affected in AS, and further studies should expand the analyses to other brain regions and behaviors.

Our results extend previous findings of an increased ARC level in AS (6, 7) by showing that IEG protein metabolism impairment, rather than ARC increase only, is associated with AS. Our findings showing lack of learning-evoked IEG increase in AS dHC following CFC partially disagrees with reports from Pastuzyn and Shepherd (7), who found ARC increase in the hippocampus of AS mice (particularly in synaptosomal fractions) after dark confinement for 24 hours followed by an exposure to enriched environment for 2 hours. Reasons for the discrepancy could be the different types of behaviors, timepoint of analysis, and age of the animals assessed. Nevertheless, our main conclusions of an enhanced stability of ARC protein in the AS brain, relative to WT controls, agree with those offered by Pastuzyn and Shepherd (7). Additionally, Mardirossian *et al.* (105) reported reduced ARC and FOS protein levels in the DG of AS mice, a result that disagrees with our data as well as data from Greer *et al.* (6) and Pastuzyn and Shepherd (7). A possible explanation for the disagreement is that Mardirossian *et al.* (105) investigated AS mice injected with 5-bromo-2-deoxyuridine (BrdU), which may have altered neural activation.

Our findings of increased levels of MTOR signaling substrates, together with a significantly increased rate of *de novo* protein synthesis in the dHC of AS mice implied that AS should have also an increase in MTOR and/or p-MTOR which, however, was not detected. MTOR or p-MTOR levels did not change also in WT mice subjected to learning, suggesting that either the time point chosen to assess the levels of training-induced proteins was not optimal for revealing MTOR/p-MTOR changes, or that these changes could not be detected via western blot. We also must consider that other mechanisms --still to be uncovered-- might be underlying the protein metabolism dysregulations in AS dHC. Nevertheless, the most plausible conclusion from our data is that AS is accompanied by a higher rate of *de novo* protein synthesis in the dHC linked to an impaired autophagic flux. We also cannot exclude that the increased level of protein synthesis may reflect a slower protein degradation rate. Further studies based on kinetics of mRNA translation, protein pulse-chase and rate of degradation should be able to shed light on these issues.

Our data agree with previous studies by Sun *et al.* (28,107), who suggested that an overactive MTOR and excessive protein synthesis contributes to the pathophysiology of AS. Their treatment of AS mice with the MTOR inhibitor rapamycin reversed the MTOR signaling overactivation, ameliorated deficits in synaptic plasticity and spine morphology, promoted actin filament remodeling, normalized ARC level in the hippocampus of AS mice, and significantly improved their CFC memory (107). Notably, rapamycin not only blocks the synthesis of a subset of proteins but also promotes autophagy in various cell-types including neurons (108), hence, we suggest that the beneficial effects of rapamycin in AS mice could be attributed to an increase in autophagy-mediated protein degradation. Our conclusion is opposed to that of Whang et al. (18), who, like us, found increased levels of MLP3B-II, but decreased level of SQSTM1, in addition to high levels of HAP1 in the cortex and cerebellum of AS mice, and interpreted these data as increased autophagy. Based on the multi-level evidence obtained in this study, we argue that an accumulation of autophagic proteins as well as of HAP1 (18) reflects an impaired rather than increased autophagy.

Because several molecules including ubiquitin and SQSTM1 are shared between the ubiquitin mediated proteasome system (UPS) and autophagy (109) and the two systems may crosstalk (110,111), we speculate that UBE3A may play an important role in both UPS and autophagy. Further studies are needed to address this link and how it may influence brain diseases.

We also suggest that the reduced levels of RAB5A and p-BECN1--proteins important for endosomal biogenesis (63,64,69)-- imply that the dHC of AS has impaired endosome biogenesis and/or trafficking, functions that together with autophagy are critical for synaptic development (89), activity-dependent synapse pruning (112), neurotransmitter release (113) and post-synaptic transmission (87). In agreement with this idea, we found that the dHC of AS mice has altered levels of both pre- and postsynaptic proteins and of proteins implicated in controlling synaptic vesicle trafficking and modulating neurotransmitter release (69,90-93,95,98-101).

Our data open the way to several outstanding questions. For example, the comprehensive profile of proteins that have an altered synthesis or degradation in AS dHC remains to

be identified. Future studies are also needed to determine whether and how these proteins change over developmental ages and the precise mechanisms of crosstalk among protein synthesis, ubiquitin-mediated degradation, autophagy, and lysosomal degradation.

Our results on AS mice add to findings on other mouse models of neurodevelopmental disorders including ASD, tuberous sclerosis, fragile X syndrome (FXS), and phosphatase and tensin homologue (PTEN) deletions, which also have impaired autophagy downstream of exaggerated MTOR activity, increased dendritic spine density, and changes in spine morphology (14,114,115), suggesting that mRNA translation linked to autophagy is a fundamental dysregulation of many neurodevelopmental disorders. Another major group of brain diseases that is associated to altered protein synthesis and autophagy is that of neurodegenerative diseases, including Alzheimer's disease, Parkinson's disease, Hungtington's disease, and amyotrophic lateral sclerosis (116,117).

In conclusion, our data showing a defective protein metabolism, and particularly impaired protein synthesis and autophagic flux along with altered levels of endosomal markers in the dHC of AS mice (Figure 9) provide a biological explanation for cognitive impairments of AS and perhaps of other neurodevelopmental disorders and neurodegenerative diseases linked to protein metabolism dysregulations. The partial recovery of behavioral and autophagy impairments provided by TAT Beclin 1 treatment, suggests that approaches that promote healthy endosomal and autophagy vesicle trafficking may help treating these diseases.

Supplementary Material

Refer to Web version on PubMed Central for supplementary material.

Acknowledgments and Disclosures

This work was supported by the Foundation for Angelman Syndrome Therapeutics (FAST)-Italia and NIH MH065635 to C.M.A. C.M.A. supervised the study. F.A., K.P. and C.M.A. designed the experiments and wrote the manuscript. F.A. and K.P. performed the experiments and analyzed data. The authors report no biomedical financial interests or potential conflicts of interest.

References

1. Kyllerman M (2013): Pediatric Neurology Part I: Chapter 32. Angelman syndrome (Vol. 111). Elsevier Inc. Chapters.
2. Bird LM (2014): Angelman syndrome: review of clinical and molecular aspects. Application of Clinical Genetics 7:93–104. [PubMed: 24876791]
3. Wallace ML, Burett AC, Weinber RJ, Philpot BD (2012): Maternal loss of Ube3a produces an excitatory/inhibitory imbalance through neuron type-specific synaptic defects. Neuron 74, 793–800. [PubMed: 22681684]
4. Buiting K, Williams C, Horsthemke B (2016): Angelman syndrome – insights into a rare neurogenetic disorder. Nat Rev Neurol 10:584–93.
5. Tan WH, Bird LM (2016): Angelman syndrome: Current and emerging therapies in 2016. American journal of medical genetics. Part C, Seminars in medical genetics 172: 384–401. [PubMed: 27860204]

6. Greer PL, Hanayama R, Bloodgood BL, Mardinly AR, Lipton DM, Flavell SW et al. (2010): The Angelman Syndrome protein Ube3A regulates synapse development by ubiquitinating arc. Cell 140: 704–716. [PubMed: 20211139]
7. Pastuzyn ED, Shepherd JD (2017): Activity-Dependent Arc Expression and Homeostatic Synaptic Plasticity Are Altered in Neurons from a Mouse Model of Angelman Syndrome. Front Mol Neurosci 10: 234. [PubMed: 28804447]
8. Chowdhury S, Shepherd JD, Okuno H, Lyford G, Petralia RS, Plath N et al. (2006): Arc/Arg3.1 interacts with the endocytic machinery to regulate AMPA receptor trafficking. Neuron 52, 445–459. [PubMed: 17088211]
9. Rial Verde EM, Lee-Osbourne J, Worley PF, Malinow R, Cline HT (2006): Increased expression of the immediate-early gene arc/arg3.1 reduces AMPA receptor-mediated synaptic transmission. Neuron 52, 461–474. [PubMed: 17088212]
10. Shepherd JD, Rumbaugh G, Wu J, Chowdhury S, Plath N, Kuhl D et al. (2006): Arc/Arg3.1 mediates homeostatic synaptic scaling of AMPA receptors. Neuron 52, 475–484. [PubMed: 17088213]
11. Hantak MP, Einstein J, Kearns RB, Shepherd JD (2021): Intercellular Communication in the Nervous System Goes Viral. Trends Neurosci 44(4):248–259. [PubMed: 33485691]
12. Sell GL, Margolis SS (2015): From UBE3A to Angelman syndrome: a substrate perspective. Front Neurosci 9:322. [PubMed: 26441497]
13. Kühnle S, Mothes B, Matentzoglu K, Scheffner M (2013): Role of the ubiquitin ligase E6AP/UBE3A in controlling levels of the synaptic protein Arc. Proc Natl Acad Sci U S A 110: 8888–8893. [PubMed: 23671107]
14. Yan J, Porch MW, Court-Vazquez B, Bennett M, Zukin RS (2018): Activation of autophagy rescues synaptic and cognitive deficits in fragile X mice. Proceedings of the National Academy of Sciences of the United States of America 115: E9707–E9716. [PubMed: 30242133]
15. Parzych KR, Klionsky DJ (2014): An overview of autophagy: morphology, mechanism, and regulation. Antioxid Redox Signal 20(3):460–73. [PubMed: 23725295]
16. Kuang E, Qi J, Ronai Z (2013): Emerging roles of E3 ubiquitin ligases in autophagy. Trends in biochemical sciences 38(9), 453–460. [PubMed: 23870665]
17. Wong YC, Holzbaur EL (2014): The regulation of autophagosome dynamics by huntingtin and HAP1 is disrupted by expression of mutant huntingtin, leading to defective cargo degradation. J Neurosci 34(4):1293–305. [PubMed: 24453320]
18. Wang T, Wang J, Wang J, Mao L, Tang B, Vanderklish PW et al. (2019): HAP1 is an in vivo UBE3A target that augments autophagy in a mouse model of Angelman syndrome. Neurobiology of disease 132: 104585. [PubMed: 31445164]
19. Hylin MJ, Zhao J, Tangavelou K, Rozas NS, Hood KN, MacGowan JS et al. (2018): A role for autophagy in long-term spatial memory formation in male rodents. Journal of neuroscience research 96(3), 416–426. [PubMed: 29230855]
20. Glatigny M, Moriceau S, Rivagorda M, Ramos-Brossier M, Nascimbeni AC, Lante F et al. (2019): Autophagy Is Required for Memory Formation and Reverses Age-Related Memory Decline. Carr Biol 29(3):435–448.
21. Pandey K, Yu XW, Steinmetz A, Alberini CM (2021): Autophagy coupled to translation is required for long-term memory. Autophagy 7:1614–1635.
22. Jiang YH, Armstrong D, Albrecht U, Atkins CM, Noebels JL, Eichele G et al. (1998): Mutation of the Angelman ubiquitin ligase in mice causes increased cytoplasmic p53 and deficits of contextual learning and long-term potentiation. Neuron 21:799–811. [PubMed: 9808466]
23. Eichenbaum H, Amaral DG, Buffalo EA, Buzsáki G, Cohen N, Davachi L (2016): Hippocampus at 25. Hippocampus 26(10):1238–49. [PubMed: 27399159]
24. Jiang Y, Tsai TF, Bressler J, Beaudet AL (1998): Imprinting in Angelman and Prader-Willi syndromes. Curr Opin Genet Dev 3:334–42.
25. Barry RJ, Leitner RP, Clarke AR, Einfeld SL (2005): Behavioral aspects of Angelman syndrome: a case control study. Am J Med Genet A 132A(1):8–12. [PubMed: 15578589]

26. Dindot SV, Antalffy BA, Bhattacharjee MB, Beaudet AL (2008): The Angelman syndrome ubiquitin ligase localizes to the synapse and nucleus, and maternal deficiency results in abnormal dendritic spine morphology. Human molecular genetics 17:111–118. [PubMed: 17940072]
27. Chamberlain SJ, Lalande M (2010): Angelman syndrome, a genomic imprinting disorder of the brain. J Neurosci 30:9958–63. [PubMed: 20668179]
28. Sun J, Liu Y, Moreno S, Baudry M, Bi X (2015): Imbalanced mechanistic target of rapamycin C1 and C2 activity in the cerebellum of Angelman syndrome mice impairs motor function. J Neurosci 35(11):4706–18. [PubMed: 25788687]
29. Sonzogni M, Wallaard I, Santos SS, Kingma J, du Mee D, van Woerden GM, Elgersma Y (2018): A behavioral test battery for mouse models of Angelman syndrome: a powerful tool for testing drugs and novel Ube3a mutants. Mol Autism 9:47. [PubMed: 30220990]
30. Miura K, Kishino T, Li E, Webber H, Dikkes P, Holmes GL, Wagstaff J (2002): Neurobehavioral and electroencephalographic abnormalities in Ube3a maternal-deficient mice. Neurobiol Dis 9(2):149–59. [PubMed: 11895368]
31. Jiang YH, Pan Y, Zhu L, Landa L, Yoo J, Spencer C et al. (2010): Altered ultrasonic vocalization and impaired learning and memory in Angelman syndrome mouse model with a large maternal deletion from Ube3a to Gabrb3. PLoS One 5(8):e12278. [PubMed: 20808828]
32. Kaphzan H, Hernandez P, Jung JI, Cowansage KK, Deinhardt K, Chao MV, Abel T, Klann E (2012): Reversal of impaired hippocampal long-term potentiation and contextual fear memory deficits in Angelman syndrome model mice by ErbB inhibitors. Biol Psychiatry 72(3):182–90. [PubMed: 22381732]
33. Huang HS, Burns AJ, Nonneman RJ, Baker LK, Riddick NV, Nikolova VD et al. (2013): Behavioral deficits in an Angelman syndrome model: effects of genetic background and age. Behav Brain Res 243:79–90. [PubMed: 23295389]
34. Dutta R, Crawley JN (2020): Behavioral Evaluation of Angelman Syndrome Mice at Older Ages. Neuroscience 445:163–171. [PubMed: 31730795]
35. Cruz E, Descalzi G, Steinmetz A, Scharfman HE, Katzman A, Alberini CM (2021): CIM6P/IGF-2 Receptor Ligands Reverse Deficits in Angelman Syndrome Model Mice. Autism Res 1:29–45.
36. Rotaru DC, Mientjes EJ, Elgersma Y (2020): Angelman Syndrome: From Mouse Models to Therapy. Neuroscience 445:172–189. [PubMed: 32088294]
37. Fanselow MS (1986): Associative vs topographical accounts of the immediate shock-freezing deficit in rats: Implication for the response selection rules governing species-specific defensive reactions. Learning and Motivation 17:16–39.
38. Steinmetz AB, Stern SA, Kohtz AS, Descalzi G, Alberini CM (2018): Insulin-Like Growth Factor II Targets the mTOR Pathway to Reverse Autism-Like Phenotypes in Mice. J Neurosci 38(4):1015–1029. [PubMed: 29217683]
39. Schmidt EK, Clavarino G, Ceppi M, Pierre P (2009): SUnSET, a nonradioactive method to monitor protein synthesis. Nature methods 6: 275–277. [PubMed: 19305406]
40. Yu XW, Pandey K, Katzman AC, Alberini CM (2020): A role for CIM6P/IGF2 receptor in memory consolidation and enhancement. Elife 9:e54781. [PubMed: 32369018]
41. Minatohara K, Akiyoshi M, Okuno H (2016): Role of Immediate-Early Genes in Synaptic Plasticity and Neuronal Ensembles Underlying the Memory Trace. Front Mol Neurosci 8:78. [PubMed: 26778955]
42. Plath N, Ohana O, Dammermann B, Errington ML, Schmitz D, Gross C et al. (2006): Arc/Arg3.1 is essential for the consolidation of synaptic plasticity and memories. Neuron 52(3):437–44. [PubMed: 17088210]
43. Alberini CM (2009): Transcription factors in long-term memory and synaptic plasticity. Physiol Rev 89 (1):121–45. [PubMed: 19126756]
44. Nakayama D, Iwata H, Teshirogi C, Ikegaya Y, Matsuki N, Nomura H (2015): Long-delayed expression of the immediate early gene Arc/Arg3.1 refines neuronal circuits to perpetuate fear memory. J Neurosci 35(2):819–30. [PubMed: 25589774]
45. Chiang GG, Abraham RT (2005): Phosphorylation of mammalian target of rapamycin (mTOR) at Ser-2448 is mediated by p70S6 kinase. J Biol Chem 280:25485–90. [PubMed: 15899889]

46. Knight ZA, Tan K, Birsoy K, Schmidt S, Garrison JL, Wysocki RW (2012): Molecular profiling of activated neurons by phosphorylated ribosome capture. Cell 151(5):1126–37. [PubMed: 23178128]
47. Biever A, Valjent E, Puighermanal E (2015): Ribosomal protein S6 phosphorylation in the nervous system: from regulation to function. Front Mol Neurosci 8:75. [PubMed: 26733799]
48. Klann E, Dever TE (2004): Biochemical mechanisms for translational regulation in synaptic plasticity. Nat Rev Neurosci 5:931–942. [PubMed: 15550948]
49. Puighermanal E, Biever A, Pascoli V, Melser S, Pratlong M, Cutando L (2017): Ribosomal Protein S6 Phosphorylation Is Involved in Novelty-Induced Locomotion, Synaptic Plasticity and mRNA Translation. Front Mol Neurosci 10:419. [PubMed: 29311811]
50. Wang X, Proud CG (2006): The mTOR pathway in the control of protein synthesis. Physiology (Bethesda) 21:362–9. [PubMed: 16990457]
51. Pause A, Belsham GJ, Gingras AC, Donzé O, Lin TA, Lawrence JC Jr, Sonenberg N (1994): Insulin-dependent stimulation of protein synthesis by phosphorylation of a regulator of 5'-cap function. Nature 371(6500):762–7. [PubMed: 7935836]
52. Iadevaia V, Liu R, Proud CG (2014): mTORC1 signaling controls multiple steps in ribosome biogenesis. Semin Cell Dev Biol 36:113–20. [PubMed: 25148809]
53. Bah A, Vernon RM, Siddiqui Z, Krzeminski M, Muhandiram R, Zhao C et al. (2015): Folding of an intrinsically disordered protein by phosphorylation as a regulatory switch. Nature 519 (7541):106–109. [PubMed: 25533957]
54. Amorim IS, Lach G and Gkogkas CG (2018): The Role of the Eukaryotic Translation Initiation Factor 4E (eIF4E) in Neuropsychiatric Disorders Front Genet 9:561. [PubMed: 30532767]
55. Evans HT, Bodea LG, Götz J. (2020): Cell-specific non-canonical amino acid labelling identifies changes in the *de novo* proteome during memory formation. Elife 9:e52990. [PubMed: 31904341]
56. Shrestha P, Klann E (2022): Spatiotemporally resolved protein synthesis as a molecular framework for memory consolidation. Trends Neurosci 45(4):297–311.. [PubMed: 35184897]
57. Costa-Mattioli M, Sossin WS, Klann E, Sonenberg N (2009): Translational control of long-lasting synaptic plasticity and memory. Neuron 61:10–26. [PubMed: 19146809]
58. Shrestha P, Ayata P, Herrero-Vidal P, Longo F, Gastone A, LeDoux JE, (2020): Cell-type-specific drug-inducible protein synthesis inhibition demonstrates that memory consolidation requires rapid neuronal translation. Nat Neurosci 23(2):281–292. [PubMed: 31959934]
59. Jung CH, Ro SH, Cao J, Otto NM, Kim DH (2010): mTOR regulation of autophagy. FEES Lett 584(7):1287–95.
60. Rabanal-Ruiz Y, Otten EG, Korolchuk VI (2017): mTORC1 as the main gateway to autophagy. Essays Biochem 61(6):565–584. [PubMed: 29233869]
61. Kim J, Kundu M, Viollet B, Guan KL (2011): AMPK and mTOR regulate autophagy through direct phosphorylation of Ulk1. Nat Cell Biol 13(2):132–41. [PubMed: 21258367]
62. Alers S, Löffler AS, Wesselborg S, Stork B (2012): Role of AMPK-mTOR-Ulk1/2 in the regulation of autophagy: cross talk, shortcuts, and feedbacks. Mol Cell Biol 32 1:2–11. [PubMed: 22025673]
63. Russell RC, Tian Y, Yuan H, Park HW, Chang YY, Kim J, (2013): ULK1 induces autophagy by phosphorylating Beclin-1 and activating VPS34 lipid kinase. Nat Cell Biol 15(7):741–50. [PubMed: 23685627]
64. McKnight NC, Zhong Y, Wold MS, Gong S, Phillips GR, Dou Z et al. (2014): Beclin 1 is required for neuron viability and regulates endosome pathways via the UVRAG-VPS34 complex. PLoS Genet 10(10):e1004626. [PubMed: 25275521]
65. Noguchi S, Honda S, Saitoh T, Matsumura H, Nishimura E, Akira S, Shimizu S (2019): Beclin 1 regulates recycling endosome and is required for skin development in mice. Commun Biol 2:37. [PubMed: 30701202]
66. Cullen PJ, Steinberg F (2018): To degrade or not to degrade: mechanisms and significance of endocytic recycling. Nat Rev Mol Cell Biol 11:679–696.
67. Simonsen A, Lippé R, Christoforidis S, Gaullier JM, Brech A, Callaghan J (1998): EEA1 links PI(3)K function to Rab5 regulation of endosome fusion. Nature 394(6692), 494–498. [PubMed: 9697774]

68. Wilson JM, de Hoop M, Zorzi N, Toh BH, Dotti CG, Parton RG (2000): EEA1, a tethering protein of the early sorting endosome, shows a polarized distribution in hippocampal neurons, epithelial cells, and fibroblasts. Mol Biol Cell 11(8):2657–71. [PubMed: 10930461]
69. Bucci C, Parton RG, Mather IH, Stunnenberg H, Simons K, Hoflack B, Zerial M (1992): The small GTPase rab5 functions as a regulatory factor in the early endocytic pathway. Cell 70(5):715–728. [PubMed: 1516130]
70. Hyttinen JM, Niittykoski M, Salminen A, Kaarniranta K (2013): Maturation of autophagosomes and endosomes: a key role for Rab7. Biochim Biophys Acta 1833(3):503–510. [PubMed: 23220125]
71. Stein SC, Woods A, Jones NA, Davison MD, Carling D (2000): The regulation of AMP-activated protein kinase by phosphorylation. Biochem J 345 Pt 3(Pt 3):437–43. [PubMed: 10642499]
72. Tanida I, Ueno T, Kominami E (2008): LC3 and Autophagy. Methods Mol Biol 445:77–88. [PubMed: 18425443]
73. Komatsu M, Ichimura Y (2010): Physiological significance of selective degradation of p62 by autophagy. FEBS letters 584(7):1374–1378. [PubMed: 20153326]
74. Liu WJ, Ye L, Huang WF, Guo LJ, Xu ZG, Wu HL, Yang C et al. (2016): p62 links the autophagy pathway and the ubiqutin-proteasome system upon ubiquitinated protein degradation. Cell Mol Biol Lett 21:29. [PubMed: 28536631]
75. Cheng XT, Xie YX, Zhou B, Huang N, Farfel-Becker T, Sheng ZH (2018): Characterization of LAMP1-labeled nondegradative lysosomal and endocytic compartments in neurons. J Cell Biol 217(9):3127–3139. [PubMed: 29695488]
76. Klionsky DJ, Abdel-Aziz AK, Abdelfatah S, Abdellatif M, Abdoli A, Abel S et al. (2021): Guidelines for the use and interpretation of assays for monitoring autophagy (4^{th} edition). Autophagy 17(1):1–382. [PubMed: 33634751]
77. Yoshii SR, Mizushima N (2017): Monitoring and Measuring Autophagy. Int J Mol Sci 18(9):1865. [PubMed: 28846632]
78. Mizushima N, Yoshimori T (2007): How to interpret LC3 immunoblotting. Autophagy 3(6):542–545. [PubMed: 17611390]
79. Ueno T, Komatsu M (2020): Monitoring Autophagy Flux and Activity: Principles and Applications. BioEssays 42(11):e2000122. [PubMed: 32851706]
80. Castillo K, Valenzuela V, Oñate M, Hetz C (2017): A Molecular Reporter for Monitoring Autophagic Flux in Nervous System In Vivo. Methods Enzymol 588:109–131. [PubMed: 28237096]
81. Baudry M, Kramar E, Xu X, Zadran H, Moreno S, Lynch G et al. (2012): Ampakines promote spine actin polymerization, long-term potentiation, and learning in a mouse model of Angelman syndrome. Neurobiol Dis 47(2):210–215. [PubMed: 22525571]
82. Kim H, Kunz PA, Mooney R, Philpot BD, Smith SL (2016): Maternal loss of Ube3a impairs experience-driven dendritic spine maintenance in the developing visual cortex. J Neurosci 36:4888–4894. [PubMed: 27122043]
83. Weeber EJ, Jiang YH, Elgersma Y, Varga AW, Carrasquillo Y, Brown SE (2003): Derangements of hippocampal calcium/calmodulin-dependent protein kinase II in a mouse model for Angelman mental retardation syndrome. J Neurosci 23(7):2634–44. [PubMed: 12684449]
84. Limbäck-Stokin K, Korzus E, Nagaoka-Yasuda R, Mayford M (2004): Nuclear calcium/calmodulin regulates memory consolidation. J Neurosci 24(48):10858–67. [PubMed: 15574736]
85. Lisman J, Yasuda R, Raghavachari S (2012): Mechanisms of CaMKII action in long-term potentiation. Nat Rev Neurosci 13(3):169–82. [PubMed: 22334212]
86. Incontro S, Díaz-Alonso J, Iafrati J, Vieira M, Asensio CS, Sohal VS, et al. (2018): Author Correction: The CaMKII/NMDA receptor complex controls hippocampal synaptic transmission by kinase-dependent and independent mechanisms. Nat Commun 9(1):5205. [PubMed: 30510185]
87. Shehata M, Matsumura H, Okubo-Suzuki R, Ohkawa N, Inokuchi K (2012): Neuronal stimulation induces autophagy in hippocampal neurons that is involved in AMPA receptor degradation after chemical long-term depression. J Neurosci 32:10413–22. [PubMed: 22836274]
88. Alvarez-Castelao B, Schuman EM (2015): The Regulation of Synaptic Protein Turnover. J Biol Chem 290(48):28623–30. [PubMed: 26453306]

89. Lieberman OJ, Sulzer D (2020): The Synaptic Autophagy Cycle. J Mol Biol 432(8):2589–2604 [PubMed: 31866297]

90. Hilfiker S, Pieribone VA, Czernik AJ, Kao H-T, Augustine GJ, Greengard P (1999): Synapsins as regulators of neurotransmitter release. Philos Trans R Soc Lond B Biol Sci 354:269–279. [PubMed: 10212475]

91. Raja MK, Preobraschenski J, Del Olmo-Cabrera S, Martinez-Turrillas R, Jahn R, Perez-Otano I, Wesseling JF (2019): Elevated synaptic vesicle release probability in synaptophysin/gyrin family quadruple knockouts. Elife 8:e40744. [PubMed: 31090538]

92. Zhang L, Zhao ZX (2006): The impact of synapsins on synaptic plasticity and cognitive behaviors. Neurosci Bull 22:63–67. [PubMed: 17684542]

93. Cesca F, Baldelli P, Valtorta F, Benfenati F (2010): The synapsins: key actors of synapse function and plasticity. Prog Neurobiol 91(4):313–348. [PubMed: 20438797]

94. Czernik AJ, Pang DT, Greengard P (1987): Amino acid sequences surrounding the cAMP-dependent and calcium/calmodulin-dependent phosphorylation sites in rat and bovine synapsin I. Proc Natl Acad Sci U S A. 84:7518–7522. [PubMed: 3118371]

95. Kim JH, Liao D, Lau LF, Huganir RL (1998): SynGAP: a synaptic RasGAP that associates with the PSD-95/SAP90 protein family. Neuron 4:683–91.

96. Cao C, Rioult-Pedotti MS, Migani P, Yu CJ, Tiwari R, Parang K, et al. (2013): Impairment of TrkB-PSD-95 signaling in Angelman syndrome. PLoS Biol 2:e1001478.

97. Korb E, Wilkinson CL, Delgado RN, Lovero KL, Finkbeiner S (2013): Arc in the nucleus regulates PML-dependent GluA1 transcription and homeostatic plasticity. Nat Neurosci 16(7):874–883. [PubMed: 23749147]

98. Migaud M, Charlesworth P, Dempster M, Webster LC, Watabe AM, Makhinson M et al. (1998): Enhanced long-term potentiation and impaired learning in mice with mutant postsynaptic density-95 protein. Nature 396(6710):433–9. [PubMed: 9853749]

99. Chen X, Levy JM, Hou A, Winters C, Azzam R, Sousa AA (2015): PSD-95 family MAGUKs are essential for anchoring AMPA and NMDA receptor complexes at the postsynaptic density. Proc Natl Acad Sci U S A 112(50):E6983–92. [PubMed: 26604311]

100. Araki Y, Zeng M, Zhang M, Huganir RL (2015): Rapid dispersion of SynGAP from synaptic spines triggers AMPA receptor insertion and spine enlargement during LTP. Neuron 85:173–189. [PubMed: 25569349]

101. Gamache TR, Araki Y, Huganir RL (2020): Twenty Years of SynGAP Research: From Synapses to Cognition. J Neurosci 40(8):1596–1605. [PubMed: 32075947]

102. Shoji-Kawata S, Sumpter R, Leveno M, Campbell GR, Zou Z, Kinch L et al. (2013): Identification of a candidate therapeutic autophagy-inducing peptide. Nature 494(7436):201–6. [PubMed: 23364696]

103. Egan DF, Chun MG, Vamos M, Zou H, Rong J, Miller CJ et al. (2105): Small Molecule Inhibition of the Autophagy Kinase ULK1 and Identification of ULK1 Substrates. Mol Cell 59(2):285–97.

104. Cioni JM, Lin JQ, Holtermann AV, Koppers M, Jakobs MAH, Azizi A, Turner-Bridger B, Shigeoka T, Franze K, Harris WA, Holt CE. Late Endosomes Act as mRNA Translation Platforms and Sustain Mitochondria in Axons. Cell. 2019 Jan 10;176(1-2):56–72.e15. [PubMed: 30612743]

105. Mardirossian S, Rampon C, Salvert D, Fort P, Sarda N (2009): Impaired hippocampal plasticity and altered neurogenesis in adult Ube3a maternal deficient mouse model for Angelman syndrome. Exp Neurol 220(2):341–8. [PubMed: 19782683]

106. Hoeffer CA, Klann E (2010): mTOR signaling: at the crossroads of plasticity, memory and disease. Trends Neurosci 33(2):67–75. [PubMed: 19963289]

107. Sun J, Liu Y, Tran J, O'Neal P, Baudry M, Bi X (2016): mTORC1-S6K1 inhibition or mTORC2 activation improves hippocampal synaptic plasticity and learning in Angelman syndrome mice. Cell Mol Life Sci 73(22):4303–4314. [PubMed: 27173058]

108. Ravikumar B, Vacher C, Berger Z, Davies JE, Luo S, Oroz LG et al. (2004): Inhibition of mTOR induces autophagy and reduces toxicity of polyglutamine expansions in fly and mouse models of Huntington disease. Nat Genet 6:585–95.

109. Lilienbaum A (2013): Relationship between the proteasomal system and autophagy. Int J Biochem Mol Biol 4(1):1–26. [PubMed: 23638318]

110. Nam T, Han JH, Devkota S, Lee HW (2017): Emerging Paradigm of Crosstalk between Autophagy and the Ubiquitin-Proteasome System. Mol Cells 40(12):897–905. [PubMed: 29237114]

111. Kocaturk NM, Gozuacik D (2018): Crosstalk Between Mammalian Autophagy and the Ubiquitin-Proteasome System. Front Cell Dev Biol 6:128. [PubMed: 30333975]

112. Tang G, Gudsnuk K, Kuo SH, Cotrina ML, Rosoklija G, Sosunov A (2014): Loss of mTOR-dependent macroautophagy causes autistic-like synaptic pruning deficits. Neuron 83(5):1131–1143. [PubMed: 25155956]

113. Hernandez D, Torres CA, Setlik W, Cebrián C, Mosharov EV, Tang G et al. (2012): Regulation of presynaptic neurotransmission by macroautophagy. Neuron 74(2):277–84. [PubMed: 22542182]

114. Zhou J, Blundell J, Ogawa S, Kwon CH, Zhang W, Sinton C et al. (2009): Pharmacological inhibition of mTORC1 suppresses anatomical, cellular, and behavioral abnormalities in neural-specific Pten knockout mice. J Neurosci 29(6):1773–83. [PubMed: 19211884]

115. Kwon CH, Luikart BW, Powell CM, Zhou J, Matheny SA, Zhang W et al. (2006): Pten regulates neuronal arborization and social interaction in mice. Neuron 50(3):377–88. [PubMed: 16675393]

116. Nixon RA (2013): The role of autophagy in neurodegenerative disease. Nat Med 19(8):983–997. [PubMed: 23921753]

117. Lee JH, Yang DS, Goulbourne CN, Im E, Stavrides P, Pensalfini A et al. (2022): Faulty autolysosome acidification in Alzheimer's disease mouse models induces autophagic build-up of Aβ in neurons, yielding senile plaques. Nat Neurosci 25(6):688–701. [PubMed: 35654956]

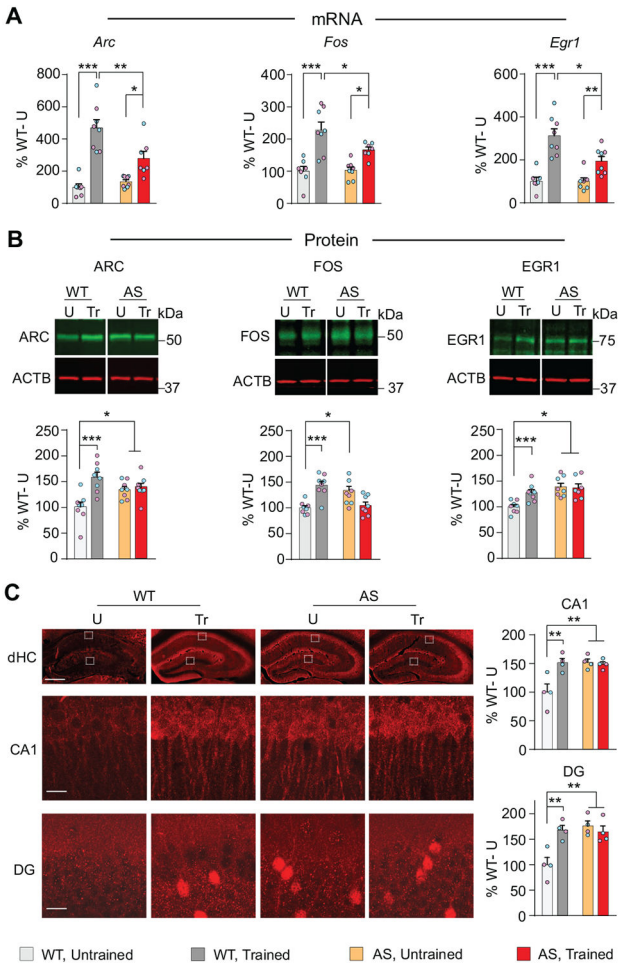

Figure 1: Increased IEGs levels in dHC of AS mice and no change following learning

(A) qPCR analyses of *Arc, Fos*, and *Egr1* mRNAs in RNA extracts from dHC of WT and AS mice trained in CFC (Tr) and euthanized 1 hour later. Control untrained mice (U) were left in their home cages and euthanized at matched timepoint. *Arc, Fos*, and *Egr1* mRNA levels were normalized to the *Gapdh* mRNA level. Data are expressed as mean percentages ± s.e.m of mean WT untrained values (WT-U = 100%). n = 7-8 mice/group, 2 independent experiments. (B) Representative western blots and relative densitometric analyses of ARC, FOS and EGR1 normalized to β-Actin (ACTB) of dHC extracts obtained from WT and AS mice trained in CFC (Tr) and euthanized 1 hour later. Control untrained mice (U) were left in their home cages and euthanized at matched timepoint. Data are expressed as mean percentages ± s.e.m of mean WT untrained values (WT-U = 100%). n = 8 mice per group, 2 independent experiments. (C) dHC images (scale bar: 500 μm) and representative confocal images of the CA1 and DG subregions (scale bar: 20 μm) obtained from WT and AS mice 1 hour after CFC (Tr), immunostained for ARC. Control untrained mice (U) were left in their home cages and euthanized at matched timepoint. Graphs represent relative quantifications of immunofluorescence intensities normalized to total number of cells (total DAPI counts). Data are expressed as mean percentages ± s.e.m of mean WT, untrained values (WT-U = 100%). n = 4 mice per group, 2 independent experiments. For each mouse, 4 images (2 per side) from 2 sections were quantified. Dots on graphs represent mean value for each mouse

(blue dots are for males and pink dots are for females). For all panels, two-way ANOVA followed by Tukey's post-hoc analysis. * $p < 0.05$, ** $p < 0.01$, *** $p < 0.001$.

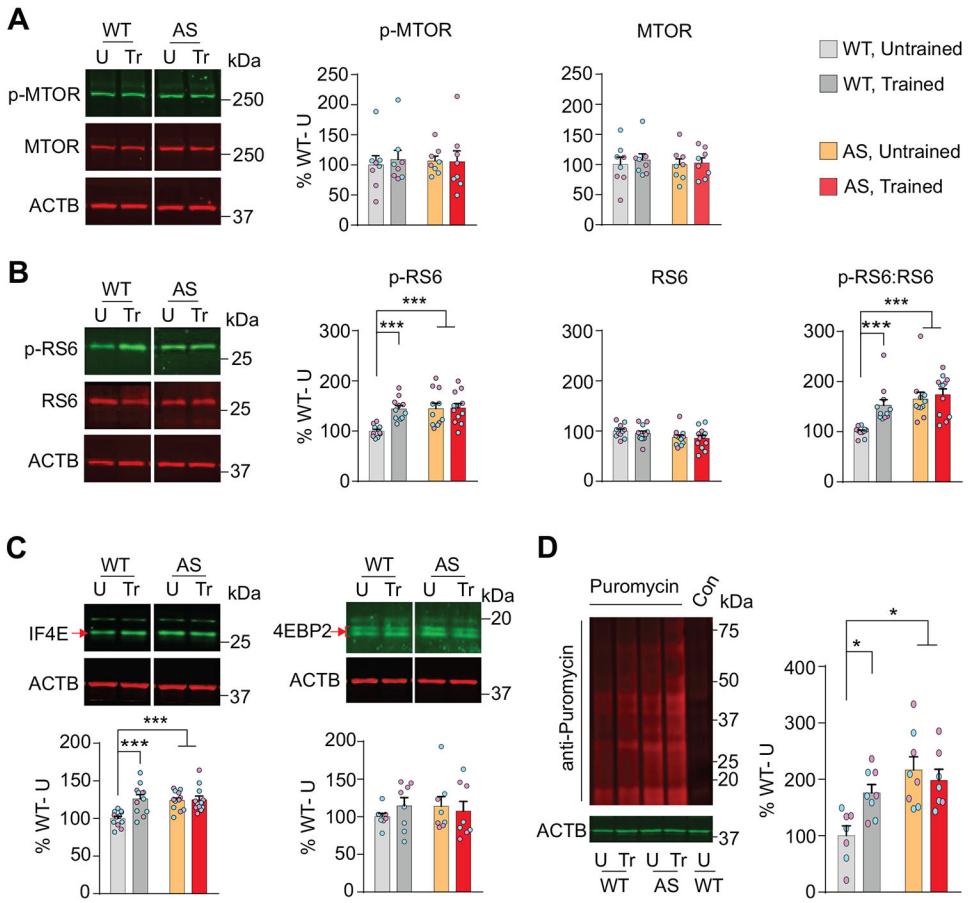

Figure 2: Overactivation of MTOR pathway and increased mRNA translation in dHC of AS mice; no change following learning

Representative western blots and relative densitometric analyses of (A) phospho-MTOR (p-MTOR), MTOR, (B) phospho-ribosomal protein S6 (p-RS6), RS6, ratio of p-RS6:RS6, (C) IF4E and 4EBP2 in dHC extracts obtained from WT and AS mice trained on CFC (Tr) and euthanized 1 hour later. Control untrained mice (U) were left in their home cages and euthanized at matched timepoint. β-Actin (ACTB) was used as loading control. Data are expressed as mean percentages ± s.e.m of mean WT untrained values (WT-U = 100%). (D) Representative western blots and relative densitometric analyses of puromycin normalized to ACTB in dHC extracts obtained from WT and AS mice bilaterally injected with puromycin 15 minutes before CFC training (Tr) and euthanized 1 hour later. A control sample without puromycin injection was included as negative control (Con). Data are expressed as mean percentages ± s.e.m of mean WT untrained values (WT-U = 100%). n = 7-12 mice per group, 2-3 independent experiments. Dots represent the mean densitometric value of each mouse (blue dots are for males and pink dots are for females). For all panels, two-way ANOVA followed by Tukey's post-hoc test. * $p < 0.05$, *** $p < 0.001$.

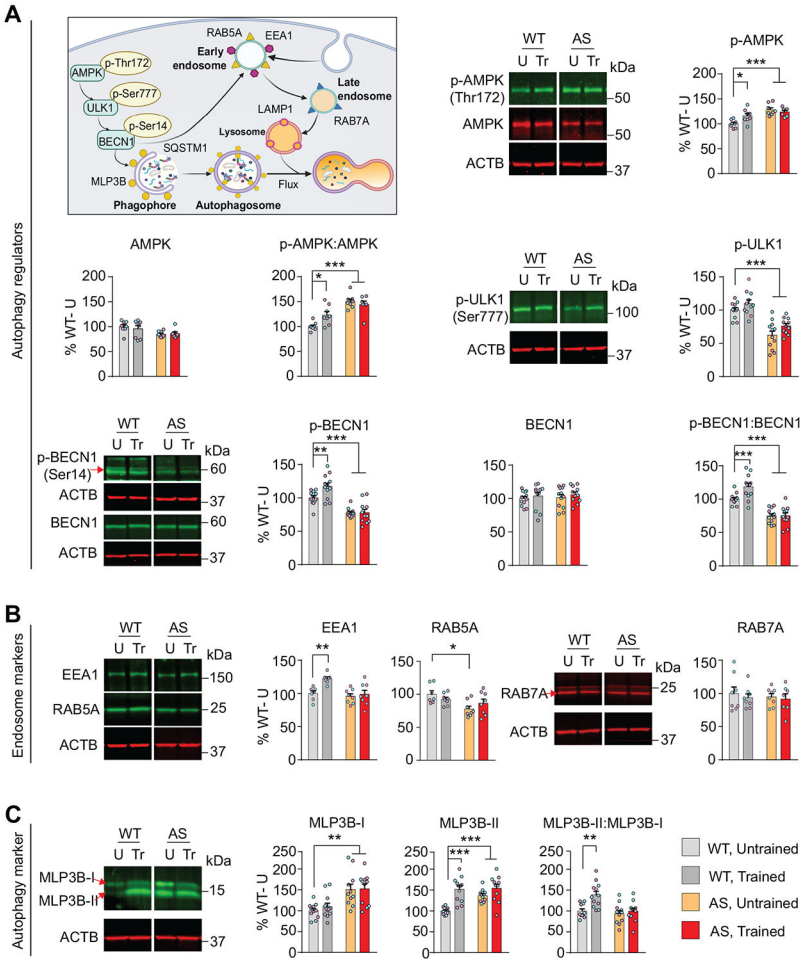

Figure 3: Accumulation of autophagy and endosome proteins in dHC of AS mice; no change following learning

(A) A schema showing major regulatory steps of autophagy and endosome pathways. Representative western blots and relative densitometric analyses of autophagy regulators and markers p-AMPK (Thr 172) and AMPK, p-AMPK:AMPK, p-ULK1 (Ser777), p-BECN1 (Ser14), BECN1, p-BECN1:BECN1, (B) markers of endosomes EEA1, RAB5A and RAB7A, and (C) MLP3B-I and MLP3B-II, and MLP3B-II:MLP3B-I in dHC extracts obtained from WT and AS mice trained on CFC (Tr) and euthanized 1 hour later. Control untrained mice (U) were left in their home cages and euthanized at matched timepoint. β-Actin (ACTB) was used as loading control. Data are expressed as mean percentages ± s.e.m of mean WT untrained values (WT-U = 100%). n =7-12 mice per group, 2-3 independent experiments. Dots represent the densitometric value of each mouse (blue dots are for males and pink dots are for females). For all panels, two-way ANOVA followed by Tukey's post-hoc analysis. * $p < 0.05$, ** $p < 0.01$, *** $p < 0.001$.

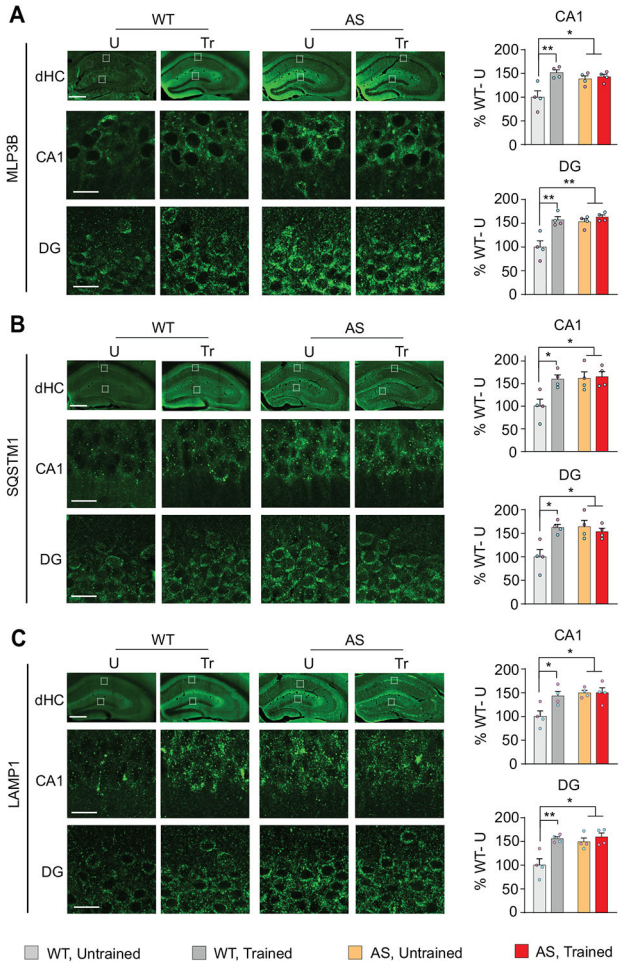

Figure 4: Accumulation of autophagy proteins in dHC of AS mice and no change following learning

dHC images (scale bar: 500 μm) and representative confocal images of the CA1 and DG subregions (scale bar: 20 μm) obtained from wild-type (WT) and AS mice 1 hour after CFC training (Tr), immunostained for (A) MLP3B (known also as LC3B), (B) SQSTM1 and (C) LAMP1. Control untrained mice (U) were left in their home cages and euthanized at matched timepoint. Graphs represent relative quantifications of total immunofluorescence intensities normalized to total number of cells (total DAPI counts). Data are expressed as mean percentages ± s.e.m of mean WT, untrained values (WT-U = 100%). n = 4 mice per group, 2 independent experiments. For each mouse, 4 images (2 per side) from 2 sections were quantified. Dots represent the mean intensity of each mouse (blue dots are for males and pink dots are for females). For all panels, two-way ANOVA followed by Tukey's post-hoc analysis. * $p < 0.05$, ** $p < 0.01$.

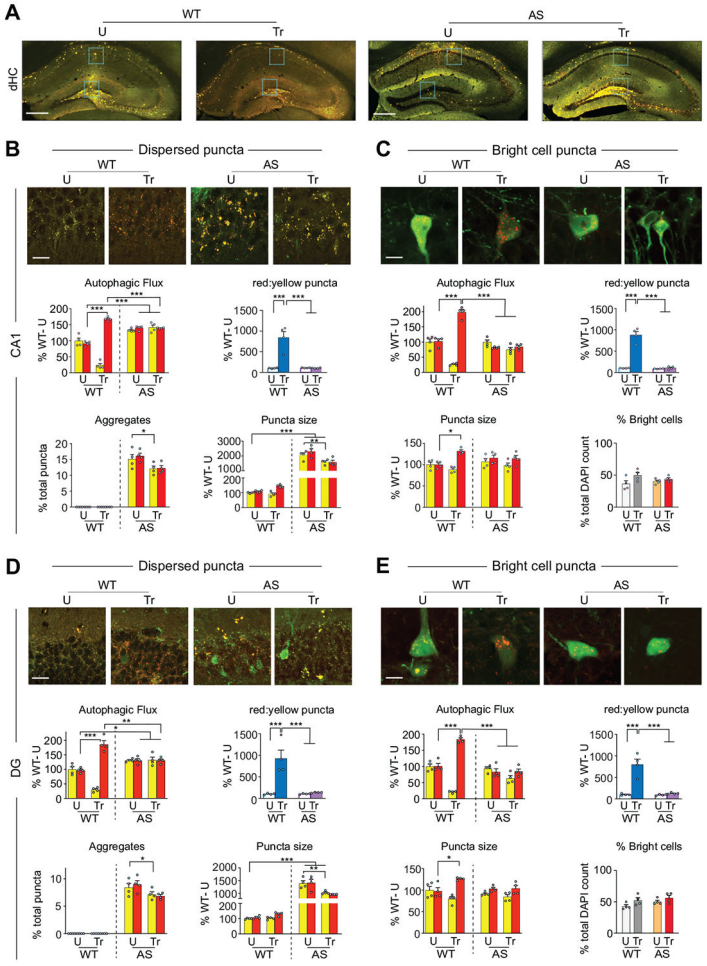

Figure 5: Impaired autophagic flux in dHC of AS mice; no change following learning

Representative images of (A) dHC (fluorescence microscopy scale bar: 500 μm), and of confocal microscopy images of (B,C) CA1 (scale bar: 20 μm) and (D,E) DG subregions. B and D show image representatives and bar graphs reporting dispersed puncta, while C and E show magnified enlargements of bright cell puncta (scale bar: 4 μm) of WT and AS mice, bilaterally injected with AAV-DJ-mCherry-GFP-LC3B into their dHC, allowed to express for two weeks, untrained or trained on CFC (Tr) and euthanized 1 hour later. The untrained (U) control mice were left in the home cage and euthanized at matched timepoint. Bar graphs report the following analyses: number of red and yellow MLP3B puncta normalized to the total number of cells (total DAPI count) (autophagic flux), the ratio of red:yellow MLP3B puncta, the average puncta size (pucta size), the percent of puncta that appears as aggregates (aggregates), and the percent of infected cells that were considered as bright cells (percent bright cells) in CA1 and DG subregions. Data are shown as mean percentages ± s.e.m. relative to the WT, untrained values (WT-U = 100%). n = 4 mice per group, 2 independent experiments. For each mouse, 4 images (2 per side) from 2 sections were quantified. Dots represent the average values for each mouse (blue dots are for males and pink dots are for females). For all panels, two-way ANOVA followed by Tukey's post-hoc analysis, except for analyses of percent of aggregates for which unpaired t-test was used. * $p < 0.05$, ** $p < 0.01$, *** $p < 0.001$.

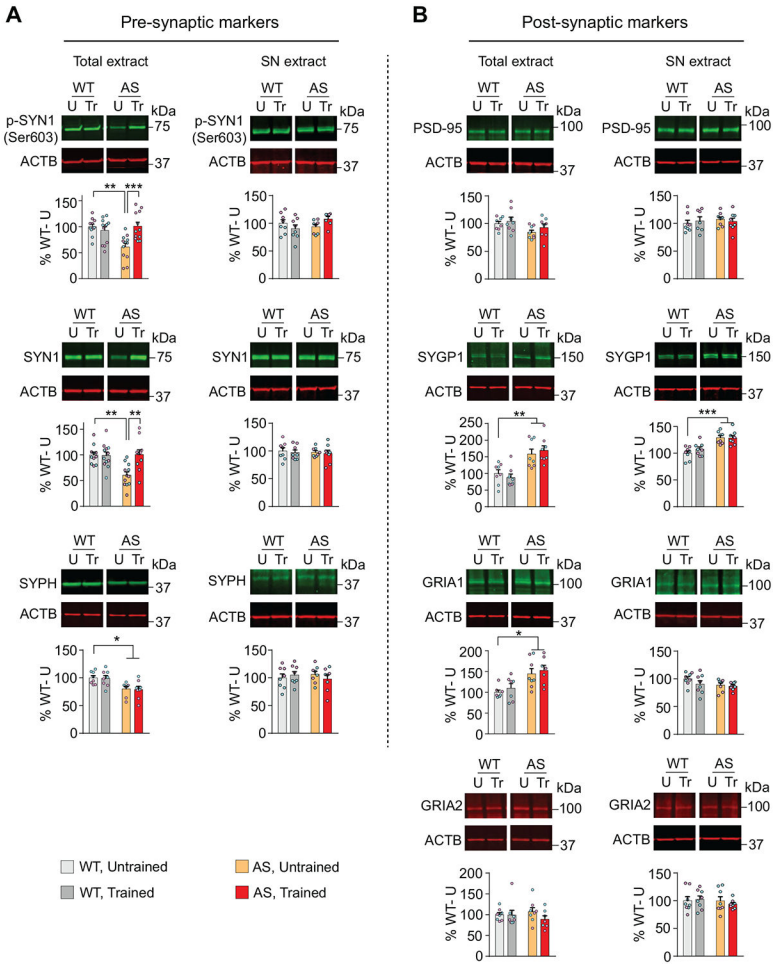

Figure 6: Altered levels of synaptic proteins in dHC of AS mice

Representative western blots and relative densitometric analyses of (A) pre-synaptic markers: p-SYN1 (Ser 603), SYN1, SYPH, and (B) post-synaptic markers: PSD-95, SYGP1, GRIA1 and GRIA2 in total protein extract and synaptoneurosomal extract obtained from dHC of WT and AS mice trained on CFC (Tr) and euthanized 1 hour later. Control untrained mice (U) were left in their home cages and euthanized at matched timepoint. β-Actin (ACTB) was used as loading control. Data are expressed as mean percentages ± s.e.m of mean WT untrained values (WT-U = 100%). n = 7-12 mice per group, 2-3 independent experiments. Dots represent the average value for each mouse (blue dots are for males and pink dots are for females). For all panels, two-way ANOVA followed by Tukey's post-hoc test. * $p < 0.05$, ** $p < 0.01$, *** $p < 0.001$.

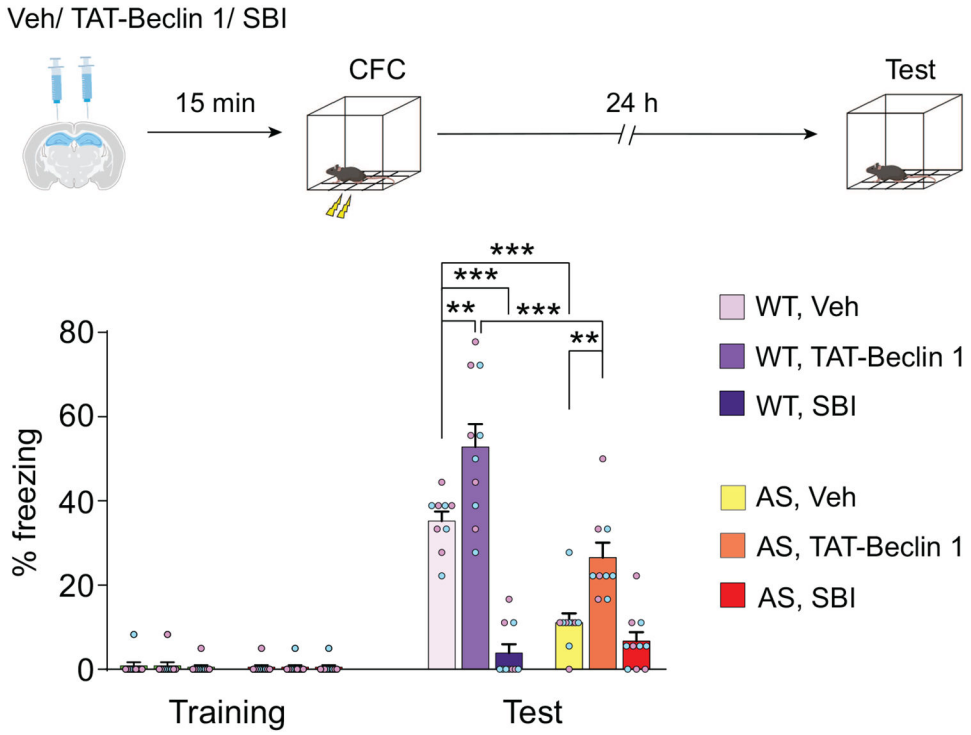

Figure 7: TAT-Beclin 1 ameliorates memory deficit in AS mice

Schematic representation of pharmacological treatment of AS and WT mice before CFC training. Mice were bilaterally injected (↓) with TAT-Beclin 1, SBI-0206965 (SBI) or vehicle (Veh) into their dHC 15 minutes (min) before CFC training and their memory retention was measured 24 hours (h) later. Memory retention is expressed as percent of time spent freezing (% freezing), n = 9-10 mice per group, 2 independent experiments. Dots represent the percent freezing value for each mouse (blue dots are for males and pink dots are for females). Two-way ANOVA followed by Tukey's post-hoc analysis. ** $p < 0.01$, *** $p < 0.001$.

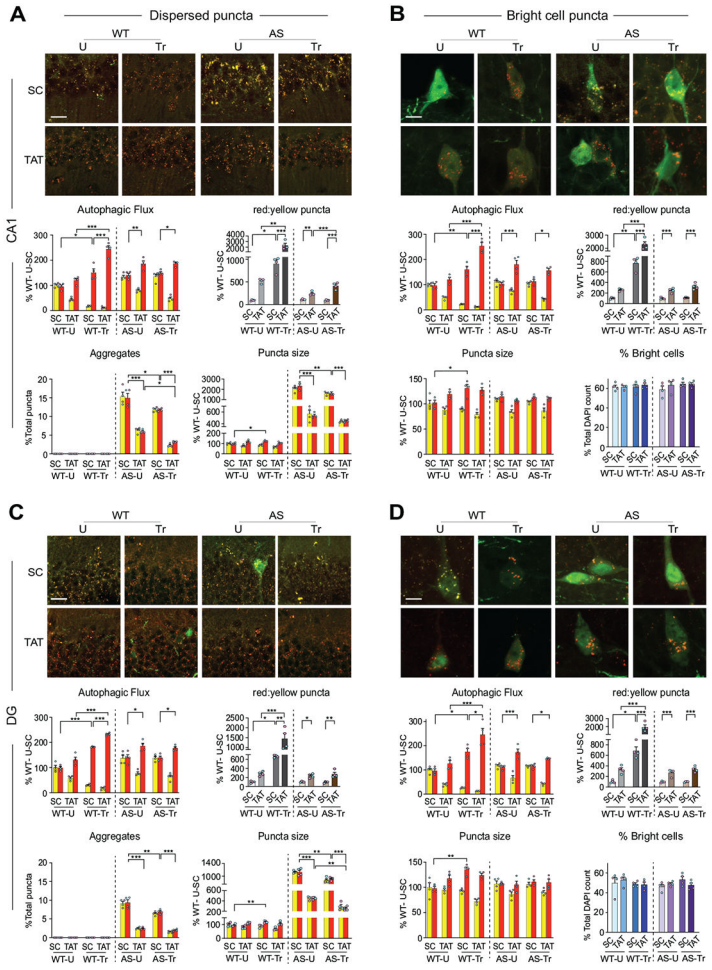

Figure 8: TAT-Beclin 1 increases autophagic flux in the dHC of AS mice

WT and AS mice were bilaterally injected into their dHC with AAV-DJ-mCherry-GFP-LC3B, allowed to express for two weeks, trained on CFC (Tr) 15 minutes (mins) after a bilateral injection of scrambled (SC) or TAT-Beclin 1 (TAT) peptide into their dHC, and euthanized 1 hour after training. Corresponding untrained (U) control mice were left in the home cage and euthanized at matched timepoint. Left: representative confocal images of (scale bar: 20 μm) of dispersed puncta in CA1 (A) and DG (C) subregions. Right panel: representative confocal images (scale bar: 4 μm) showing bright cell puncta in CA1 (B) and DG (D) subregions. Bar graphs showing: number of red and yellow MLP3B puncta normalized to the total number of cells (total DAPI count) (autophagic flux), the ratio of red:yellow MLP3B puncta, the average puncta size (puncta size), the percent of puncta that appears as aggregates (aggregates), and the percent of infected cells that were considered as bright cells (percent bright cells) in CA1 and DG subregions. Data are shown as mean percentages ± s.e.m. relative to the WT, scrambled-injected untrained values (WT-U-SC = 100%). n = 4 mice per group, 2 independent experiments. For each mouse, 4 images (2 per side) from 2 sections were quantified. Dots represent the average values for each mouse (blue dots are for males and pink dots are for females). For all panels, two-way ANOVA followed by Tukey's post-hoc analysis * $p < 0.05$, ** $p < 0.01$, *** $p < 0.001$.

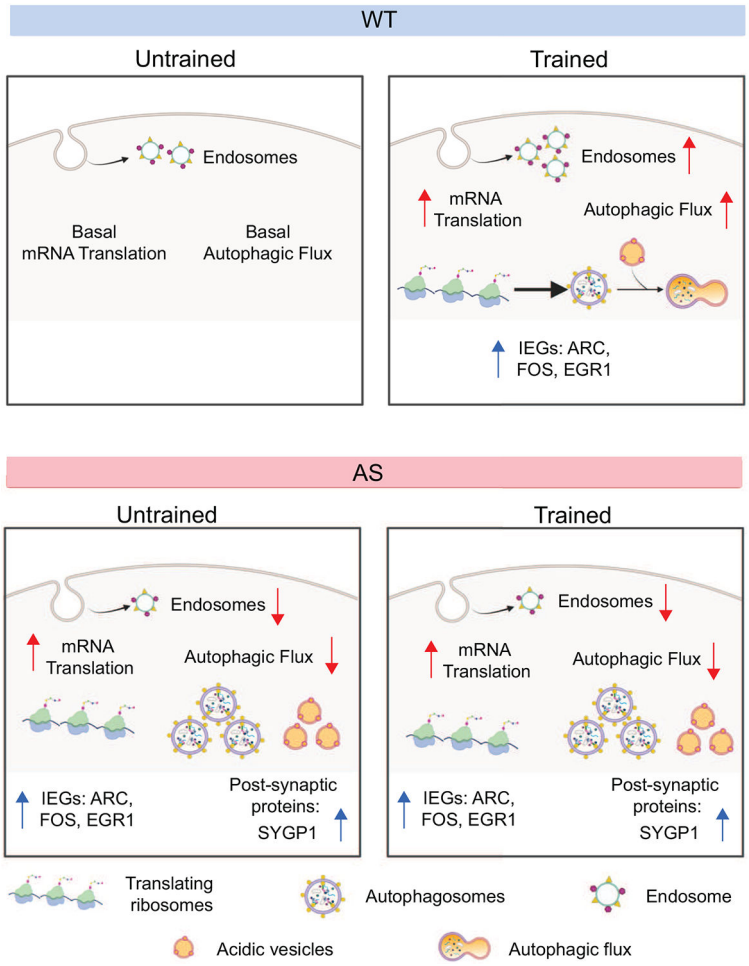

Figure 9: A model illustrating protein metabolism regulation in the dHC of WT and AS mice under basal conditions and following learning.

Under basal conditions (untrained), AS mice exhibit increased levels of *de novo* mRNA translation and impaired autophagic flux. These alterations lead to accumulation of autophagic proteins (which typically are degraded via autophagy) as well as of proteins critical for brain plasticity, including ARC, FOS and EGR1. Learning in WT mice (trained), as expected, significantly increases mRNA translation, hence *de novo* protein synthesis, including the synthesis of IEGs and of endosomal markers. This increase in endosomal markers suggest an increase in endosomes. The learning-induced increase in protein synthesis is coupled to an increase in autophagic flux. In contrast, in AS mice, learning fails to produce any change in *de novo* protein synthesis as well as in IEGs and autophagy protein levels, which remain accumulated like in untrained mice. Furthermore, the autophagic flux is impaired in AS dHC and there is a significant accumulation of autophagosomal structures, suggesting an impaired protein degradation. We propose that an altered protein metabolism in the brain due to an increased rate of protein synthesis and impaired autophagy with a lack of stimulus-dependent dynamic regulation is a critical biological alteration associated with AS. Arrows pointing up or down indicate increased or decreased levels, respectively.

KEY RESOURCES TABLE

Resource Type	Specific Reagent or Resource	Source or Reference	Identifiers	Additional Information
Add additional rows as needed for each resource type	Include species and sex when applicable.	Include name of manufacturer, company, repository, individual, or research lab. Include PMID or DOI for references; use “this paper” if new.	Include catalog numbers, stock numbers, database IDs or accession numbers, and/or RRIDs. RRIDs are highly encouraged; search for RRIDs at https://scicrunch.org/resources.	Include any additional information or notes if necessary.
Antibody	Rabbit anti-LC3B	Cell Signaling Technology (PMID:32501746)	Cat# 2775, RRID:AB_915950	1:1000
Antibody	Mouse monoclonal anti-ACTB/actin	Santa Cruz Biotechnology (PMID:18698599)	Cat# sc-47778 HRP, RRID:AB_2714189	1:15000
Antibody	Rabbit polyclonal anti-phospho (Ser2448)-mTOR	Cell Signaling Technology (PMID:24064360)	Cat# 2971, RRID:AB_330970	1:1000
Antibody	Mouse monoclonal anti-mTOR	Cell Signaling Technology (PMID:33124469)	Cat# 4517, RRID:AB_1904056	1:1000
Antibody	Rabbit polyclonal anti-phospho-S6 Ribosomal protein	Cell Signaling Technology (PMID:28017544)	Cat# 2215, RRID:AB_331682	1:1000
Antibody	Mouse monoclonal anti-RS6/S6 ribosomal protein	Novus Biologicals (PMID:29440634)	Cat# MAB5436, RRID:AB_2269697	1:1000
Antibody	Rabbit monoclonal anti-eIF4E	Cell Signaling Technology (PMID:25057190)	Cat# 2067, RRID:AB_2097675	1:1000
Antibody	Rabbit monoclonal anti-4EBP2	Cell Signaling Technology (PMID:28890345)	Cat# 2845, RRID:AB_10699019	1:1000
Antibody	Mouse monoclonal anti-Puromycin antibody	Millipore Sigma (PMID:25186761)	Cat# MABE343, RRID:AB_2566826	1:2000
Antibody	Rabbit polyclonal anti-ARC	Synaptic Systems (PMID:21456007)	Cat# 156 003, RRID:AB_887694	1:2000
Antibody	Rabbit polyclonal anti-c-FOS	Cell Signaling Technology (PMID:27545712)	Cat# 4384, RRID:AB_2106617	1:2000
Antibody	Rabbit monoclonal anti-EGR1	Thermo Fisher Scientific (PMID:23054680)	Cat# MA5-15008, RRID:AB_10977090	1:1000
Antibody	Rabbit polyclonal anti-phospho-ULK1 Antibody (Ser777)	Millipore	Cat# ABC213, RRID:AB_2861423	1:500
Antibody	Rabbit monoclonal phospho-Beclin-1 (Ser14 mouse)	Cell Signaling Technology (PMID:31400850)	Cat# 84966, RRID:AB_2800045	1:500
Antibody	Rabbit monoclonal anti-BECN1	Abcam (PMID:29367610)	Cat# ab207612, RRID:AB_2692326	1:1000
Antibody	Rabbit polyclonal anti-EEA1	Abcam (PMID:28910634)	Cat# ab2900, RRID:AB_2262056	1:1000
Antibody	Rabbit polyclonal anti-RAB5A	Abcam (PMID:28408870)	Cat# ab18211, RRID:AB_470264	1:1000
Antibody	Mouse monoclonal anti-RAB7A	Abcam (PMID:28666573)	Cat# ab137029, RRID:AB_2629474	1:1000
Antibody	Rabbit polyclonal anti-phospho (Ser603)-Synapsin I	Sigma Aldrich (PMID:12237306)	Cat# S8192, RRID:AB_261560	1:1000
Antibody	Rabbit monoclonal anti-Synapsin I	EMD Millipore, AB1543P	Cat# ab32532, RRID:AB_778198	1:5000
Antibody	Rabbit monoclonal anti-Synapmiddlehysin	Abcam (PMID:28648365)	Cat# ab32127, RRID:AB_2286949	1:5000

Resource Type	Specific Reagent or Resource	Source or Reference	Identifiers	Additional Information
Antibody	Mouse monoclonal anti-PSD-95	Thermo Scientific (PMID:10488080)	Cat# MA1-045, RRID:AB_325399	1:1000
Antibody	rabbit monoclonal anti- AMPA receptor 1 (GluA1)	Cell Signaling Technology (PMID:30249796)	Cat# 13185, RRID:AB_2732897	1:1000
Antibody	mouse monoclonal anti-GLUR2	NeuroMab (PMID:17656725)	Cat# 75-002, RRID:AB_2232661	1:500
Antibody	rabbit monoclonal anti-SYNGAP	Abcam (PMID:31939740)	Cat# ab77235, RRID:AB_1524465	1:1000
Antibody	Rabbit polyclonal anti-ACTB/actin	Santa Cruz Biotechnology (PMID:18698599)	Cat# sc-1616, RRID:AB_630836	1:20000
Antibody	Goat polyclonal anti-rabbit IRDye® 800CW	LI-COR (PMID:24456162)	Cat# 926-32211, RRID:AB_621843	1:15000
Antibody	Goat polyclonal anti-mouse IRDye® 680LT	LI-COR (PMID:26994698)	Cat# 926-68020, RRID:AB_10706161	1:15000
Antibody	Mouse monoclonal anti-LC3B	Enzo Life Sciences (PMID:32501746)	Cat# ALX-803-080-C100, RRID:AB_2051773	1:500
Antibody	Guinea pig polyclonal anti-SQSTM1/p62	American Research Products (PMID:25855184)	Cat# 03-GP62-C, RRID:AB_1542690	1:1000
Antibody	Mouse monoclonal anti-LAMP1	Novus Biologicals (PMID: 34359852)	Cat# NBP2-52721	1:2000
Antibody	Goat polyclonal anti-rabbit Alexa Fluor 488	Thermo Fisher Scientific (PMID:28283064)	Cat# A32731, RRID:AB_2633280	1:1000
Antibody	Goat polyclonal anti-guinea pig Alexa Fluor 488	Invitrogen (PMID:10924501)	Cat# A-11073, RRID:AB_2534117	1:1000
Antibody	Goat polyclonal anti-rabbit Alexa Fluor 647	Thermo Fisher Scientific (PMID:28384468)	Cat# A32733, RRID:AB_2633282	1:1000
Antibody	Goat polyclonal anti-mouse Alexa Fluor 488	Thermo Fisher Scientific (PMID:28475896)	Cat# A32723, RRID:AB_2633275	1:1000
Antibody	Mouse anti-AMPKa	Cell Signaling (PMID:23653460)	Cat# 2793, RRID:AB_915794	1:1000
Antibody	rabbit anti- phospho-AMPKα (Thr172)	Cell Signaling (PMID:23709089)	Cat#2535,RRID:AB_331250	1:1000
Antibody	Rabbit monoclonal anti-MAP2	Abcam (PMID: 34080759)	Cat# ab183830, RRID: AB_2895301	1:5000
Bacterial or Viral Strain	AAV-DJ-mCherry-GFP-LC3	Stanford University Gene Vector and Virus Core	N/A	5.79×10^{12} Vg/ml
Biological Sample	N/A			
Cell Line	N/A			
Chemical Compound or Drug	Pierce Protease and Phosphatase Inhibitor Mini Tablets	Thermo Scientific	Cat# A32959	
Chemical Compound or Drug	Prolong Diamond antifade mountant with DAPI	Invitrogen	Cat# P36962	
Chemical Compound or Drug	TAT-Beclin 1	Sigma Aldrich (PMID: 30661803)	Cat# T1331	
Chemical Compound or Drug	SBI 0206965	Sigma Aldrich (PMID:32501746)	Cat# SML1540	

Resource Type	Specific Reagent or Resource	Source or Reference	Identifiers	Additional Information
Chemical Compound or Drug	SYBR® Green Master Mix	Bio-Rad	Cat# 170-8882	
Chemical Compound or Drug	QIAzol Lysis Reagent	Qiagen	Cat# 79306	
Commercial Assay Or Kit	RNeasy Plus Universal Mini Kit	Qiagen	Cat# 73404	
Deposited Data; Public Database	N/A			
Genetic Reagent	N/A			
Organism/Strain	Mouse: B6.129S7-Ube3atm1Alb/J, male and female	The Jackson Laboratory	RRID:IMSR_JAX:016590	
Organism/Strain	Mouse: C57BL/6J, male and female	The Jackson Laboratory	RRID:IMSR_JAX:000664	
Peptide, Recombinant Protein	N/A			
Recombinant DNA	N/A			
Sequence-Based Reagent	Primers fo q-PCR see Supplement 1, Material and Methods, RNA extraction and qPCR analysis	This paper		
Software; Algorithm	GraphPad Prism software 9	GraphPad Software Inc.		
Software; Algorithm	ImageJ software 1.41	ImageJ		
Software; Algorithm	Leica Application Suite X (LAS X) software	Leica microsystems		
Software; Algorithm	Image Studio™ Lite Software	LI-COR		
Software; Algorithm	CFX Maestro Software	Bio-Rad	Compatible with CFX96 Touch Real-Time PCR Detection System from Bio-Rad	
Transfected Construct	N/A			
Other	N/A			